Journal of Geodynamics 102 (2016) 83–94

Contents lists available at ScienceDirect

Journal of Geodynamics

journal homepage: http://www.elsevier.com/locate/jog

Absolute gravity observations in Norway (1993–2014) for glacial isostatic adjustment studies: The influence of gravitational loading effects on secular gravity trends

Vegard Ophaug[a,*], Kristian Breili[a,b], Christian Gerlach[a,c], Jon Glenn Omholt Gjevestad[a], Dagny Iren Lysaker[b], Ove Christian Dahl Omang[b], Bjørn Ragnvald Pettersen[a]

[a] Department of Mathematical Sciences and Technology, Norwegian University of Life Sciences (NMBU), Ås, Norway
[b] Geodetic Institute, Norwegian Mapping Authority, Hønefoss, Norway
[c] Commission of Geodesy and Glaciology, Bavarian Academy of Sciences and Humanities, Munich, Germany

ARTICLE INFO

Article history:
Received 16 April 2016
Received in revised form 4 August 2016
Accepted 10 September 2016
Available online 24 September 2016

Keywords:
Absolute gravity
Ocean tide loading
Non-tidal ocean loading
Atmospheric effect
Global hydrological effect
Time-variable gravity
Land uplift
Glacial isostatic adjustment
Gravity-to-height ratios

ABSTRACT

We have compiled and analyzed FG5 absolute gravity observations between 1993 and 2014 at 21 gravity sites in Norway, and explore to what extent these observations are applicable for glacial isostatic adjustment (GIA) studies. Where available, raw gravity observations are consistently reprocessed. Furthermore, refined gravitational corrections due to ocean tide loading and non-tidal ocean loading, as well as atmospheric and global hydrological mass variations are computed. Secular gravity trends are computed using both standard and refined corrections and subsequently compared with modeled gravity rates based on a GIA model. We find that the refined gravitational corrections mainly improve rates where GIA, according to model results, is not the dominating signal. Consequently, these rates may still be considered unreliable for constraining GIA models, which we trace to continued lack of a correction for the effect of local hydrology, shortcomings in our refined modeling of gravitational effects, and scarcity of observations. Finally, a subset of standard and refined gravity rates mainly reflecting GIA is used to estimate ratios between gravity and height rates of change by ordinary and weighted linear regression. Relations based on both standard and refined gravity rates are within the uncertainty of a recent modeled result.

1. Introduction

Gravimetry considers the observation or measurement of gravity. It may be spaceborne, air- and shipborne, or ground-based (terrestrial), where latter observations may be used to validate results from the first (e.g., Šprlák et al., 2015). Observing temporal gravity changes, and thus changes in the Earth's density distribution, gives insight into a range of geophysical phenomena, e.g., Earth tides, Chandler wobble, core, mantle and tectonic processes (Torge and Müller, 2012), sea-level change (e.g., Simpson et al., 2013), the hydrological cycle (e.g., Pálinkáš et al., 2012), and cryospheric mass variations (e.g., Breili and Rolstad, 2009; Arneitz et al., 2013). Long-term temporal gravity changes can be observed by repeated absolute gravimetry, with an accuracy of ~0.5 μGal yr^{-1} (where 1 μGal = 10^{-8} ms^{-2}) after 10 years of annual observations (Van Camp et al., 2016).

As opposed to space-geodetic observation techniques such as Global Navigation Satellite Systems (GNSS), absolute gravity (AG) is independent of the terrestrial reference frame, and may thus be used to assess it (e.g., Mazzotti et al., 2011; Collilieux et al., 2014). Furthermore, AG is particularly suitable for monitoring long-term vertical deformation (Van Camp et al., 2011) caused by, e.g., glacial isostatic adjustment (GIA) in North America (e.g., Lambert et al., 2006) and Fennoscandia (e.g., Steffen et al., 2009; Pettersen, 2011; Müller et al., 2012; Timmen et al., 2011, 2015; Nordman et al., 2014), alongside GNSS (e.g., Milne et al., 2001; Vestøl, 2006).

Sasagawa (1989) reviewed the required time span of gravity observations for determining a secular gravity trend with desired accuracy, given by

$$\sigma_{\dot{g}} = \frac{\sigma_g \sqrt{12}}{T\sqrt{N - \frac{1}{N}}}, \tag{1}$$

where $\sigma_{\dot{g}}$ is the trend uncertainty, σ_g is the uncertainty of individual gravity observations, T is the time in years, and N the number of observations. Eq. (1) assumes evenly distributed observations with known uncertainties and a true Gaussian distribution. Steffen

* Corresponding author.
E-mail address: vegard.ophaug@nmbu.no (V. Ophaug).

http://dx.doi.org/10.1016/j.jog.2016.09.001

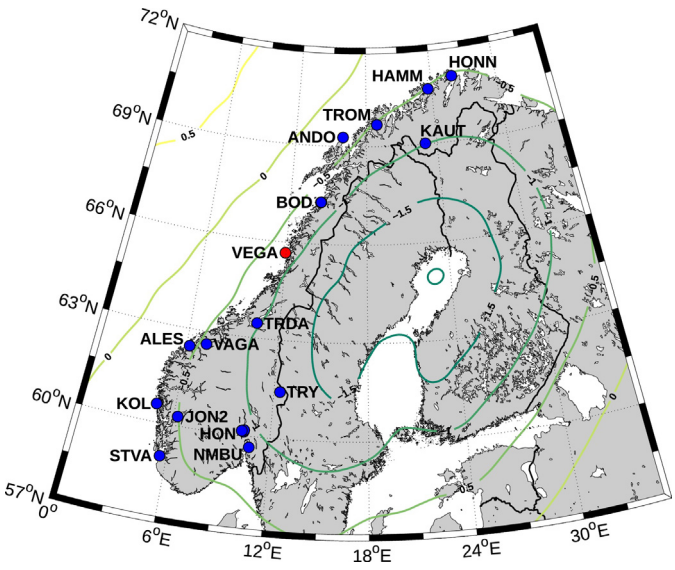

Fig. 1. AG sites in Norway. Blue sites have been observed more than once. The contour lines show modeled gravity rates (μGal yr^{-1}) from the preliminary NKG2016GIA_prel0306 GIA model (H. Steffen, personal communication, 2016). (For interpretation of the references to colour in this figure legend, the reader is referred to the web version of this article.)

and Wu (2011) further state that a secular gravity trend should be known within an uncertainty of $\pm 0.5\,\mu$Gal yr^{-1} for crustal deformation studies, which, by Eq. (1), should be achieved by five to six years of annual gravity observations with $\sigma_g \approx 1-2\,\mu$Gal.

In 1990, the Nordic Geodetic Commission (NKG, http://www.nordicgeodeticcommission.com/) began establishing a geodetic network for monitoring crustal deformations and sea-level changes in Fennoscandia and Svalbard. As part of this initiative, the first AG observations with modern instruments were performed in Norway in 1991 and 1992 (Roland, 1998). Between 1991-1995, several AG campaigns were conducted in Fennoscandia and Svalbard (Roland, 1998).

Breili et al. (2010) established an AG reference frame for Norway including 16 gravity sites. Since then, it has been extended to include 21 sites, as shown in Fig. 1 and Table 1. Gravity sites marked in blue have been observed more than once, thus only VEGA is excluded from the set of candidates for trend computation. There exist single observations at a few other sites, but these are less likely to be revisited and are therefore not considered in our work. The observation time spans are ~5 years or longer for 18 of the 21 sites (Table 1). Unfortunately, some gravity sites show uneven observation distributions, with typically larger gaps between initial and later observations. Thus we interpret Eq. (1) as a best-case scenario for our data sets.

The present crustal movements of Fennoscandia are largely due to the viscoelastic process of GIA (or postglacial rebound), which has been monitored by geodetic techniques (e.g., Milne et al., 2001; Lidberg et al., 2010; Kierulf et al., 2014; Steffen and Wu, 2011). The GIA pattern of Fennoscandia is shown in Fig. 1.

This work presents results from two decades of AG observations in Norway, and an attempt is made to derive empirical secular gravity trends based on these data. Our main goal is to explore to what extent the gravity trends are applicable for GIA studies. A prerequisite for this goal is a homogenization of the gravity trends through a consistent analysis of the AG data. This is done by investigating to what extent the gravity trends reflect GIA or other geophysical processes. Ideally, careful reduction of other geophysical processes will ultimately give the pure GIA signal. Therefore, we compute refined ocean loading, atmospheric, and global hydrological effects on gravity, and explore how these affect the trends. Finally, the relation between gravity and height rates of change is investigated. The presented gravity values serve as a Norwegian contribution to the Fennoscandian AG project of the Working Group on Geodynamics of the NKG, which aims to combine all Fennoscandian AG data in a joint analysis on postglacial gravity change for the region.

Section 2 covers fundamentals of the AG processing scheme, where Sections 2.1 and 2.2 concern the refined modeling of ocean, atmospheric and hydrological effects on gravity. Secular gravity trends are computed in Section 3, and a subset of reliable trends are used for determining ratios between the rates of change of gravity and height. Results are discussed in Section 4, while Section 5 concludes the work with recommendations for future AG observations in Norway.

2. Processing absolute gravity

All AG observations in this work were made with the FG5 (Niebauer et al., 1995) absolute gravimeter, which has an accuracy of 1–2 μGal. It is ballistic, i.e., it applies the free-fall principle, where a test mass is dropped in vacuum. A laser interferometer and atomic clock are used to obtain time-distance pairs, and Newton's equations of motion are solved to obtain the acceleration. A typical observation campaign lasts 1–2 days, including several hourly gravity sets where a set consists of 50-100 drops of the test mass. With few exceptions, we have used observations made during the same season (between May and September), so as to reduce seasonal effects (e.g., the influence of surface snow cover during winter).

To minimize computational biases, we have adopted a common processing scheme for the data analysis, ensuring consistency with respect to model and setup parameters. All raw gravity observations have been reprocessed using the g9 software (Micro-g LaCoste, 2012), developed by Micro-g LaCoste and bundled with the instrument.

Vertical transfer of the measured gravity value is done using the vertical gravity gradient, which has been determined at each gravity site using the LaCoste & Romberg G-761 relative gravimeter, see Table 1. All AG observations in this work are given at a reference height of 120 cm, close to a point where the influence of the gradient uncertainty on the FG5 is almost zero (Timmen, 2010).

The most important time-variable components of the raw gravity value are reduced in the software by various models, i.e., variations due to solid Earth and ocean tides, polar motion, ocean loading, and atmospheric mass (Timmen, 2010). The atmospheric correction is determined by observed barometric pressure during the observations, which was done at all sites except Hammerfest in 2006.488, where the barometer failed, and pressure observations transferred from a nearby weather station were used instead (Breili et al., 2010). Corrections for polar motion were computed using final polar coordinates from the International Earth Rotation and Reference Systems Service (IERS), at http://datacenter.iers.org.

The bulk of observations presented here were made with the FG5-226 AG meter of the Norwegian University of Life Sciences (NMBU). The rubidium (Rb) frequency standard of the FG5-226 has been calibrated (i.e., compared with a stable reference signal) at convenience since its acquisition in April 2004, and on a regular basis using a portable Rb reference since the oscillator was replaced in May 2007. We have observed it to vary within a range of ~0.02 Hz (where 0.01 Hz roughly corresponds to 2 μGal). While Gitlein (2009) reports a linear drift of the FG5-220 Rb frequency, the FG5-226 Rb frequency development is non-linear, see Fig. 2. A stable frequency was observed with the original oscillator, while the frequency changed by ~−0.005 Hz during the first year after its replacement. Then it was stable within 0.002 Hz until a large

Table 1
Absolute gravity sites in Norway, gravity gradients, and observation spans.

Site	Code	φ (°)	λ (°)	H (m)	$\partial g/\partial H$[a] (μGal cm^{-1})	t_g[b] (yrs)	n_g[c]
Andøya	ANDO	69.278	16.009	370	−4.04 ± 0.01	6.0	5
Bodø Asylhaugen	BODB	67.288	14.434	68	−3.31 ± 0.01	4.0	4
Bodø Bankgata	BODA	67.280	14.395	13	−2.64 ± 0.02	5.1	4
Hammerfest	HAMM	70.662	23.676	17	−3.14 ± 0.01	4.0	2
Honningsvåg	HONN	70.977	25.965	20	−3.54 ± 0.01	4.9	5
Hønefoss AA	HONA	60.124	10.364	108	−2.23 ± 0.04	16.7	2
Hønefoss AB	HONB	60.167	10.389	604	−3.11 ± 0.02	16.7	4
Hønefoss AC	HONC	60.143	10.250	120	−2.80 ± 0.02	15.9	12
Jondal 2	JON2	60.286	6.246	52	−2.53 ± 0.03	9.0	2
Kautokeino	KAUT	69.022	23.020	388	−3.08 ± 0.01	4.9	5
Kollsnes 1	KOL1	60.559	4.836	10	−2.67 ± 0.01	7.7	2
Kollsnes 2	KOL2	60.557	4.828	3	−2.80 ± 0.02	7.7	2
Stavanger AA	STVA	59.018	5.599	55	−2.86 ± 0.08	15.2	7
Tromsø	TROM	69.663	18.940	103	−3.34 ± 0.01	15.9	8
Trondheim AA	TRDA	63.455	10.446	27	−2.95 ± 0.01	14.8	10
Trysil AB	TRYB	61.423	12.381	693	−3.85 ± 0.01	16.8	7
Trysil AC	TRYC	61.423	12.381	693	−3.85 ± 0.01	18.0	17
Vågstranda AA	VAGA	62.613	7.275	38	−3.03 ± 0.01	7.2	4
Vega	VEGA	65.673	11.964	12	−3.44 ± 0.01	–	1
Ålesund	ALES	62.476	6.199	145	−2.90 ± 0.01	7.0	5
Ås NMBU	NMBU	59.666	10.778	95	−2.94 ± 0.01	9.9	10

[a] Determined by repeated observations of the gravity difference between the floor marker and ∼1.4 m above it.
[b] Number of years.
[c] Number of campaigns.

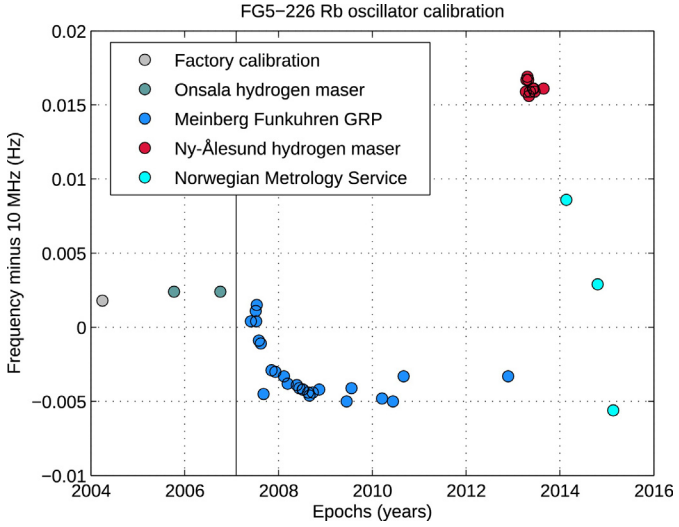

Fig. 2. Calibration of the FG5-226 Rb oscillator. The vertical bar denotes the oscillator replacement (May 2007).

frequency offset of ∼0.02 Hz was observed during the 2013 campaign in Ny-Ålesund in Svalbard. This large offset was due to a helium leakage from the co-located superconducting gravimeter which penetrated the Rb cell. Subsequent frequency calibrations indicate that it has slowly returned to the level prior to the helium contamination. Mäkinen et al. (2015) discuss the effect of helium contamination on Rb frequency references, and underline that large offsets are unproblematic as long as they are known and corrected for. For every observation epoch we have chosen to use the calibrated frequency value closest in time.

We have also used AG observations performed by other agencies and instruments, see Table 2. Raw observations by LM at TRYB, TRYC and VAGA in 2007 have been reprocessed using the above procedure. Observations by IfE and BKG, reported in Gitlein (2009), are given at 120 cm and 125 cm reference heights, respectively. Remaining observations by NOAA and BKG, reported in Roland (1998), are given at a reference height of 100 cm. When needed, the observations were transferred to the 120 cm reference height in two steps. First, the original gradient value was used to transfer gravity from the original reference height (100 or 125 cm) to the actual measurement height. In turn, the new gravity gradients presented in this work (Table 1) were used to transfer gravity from the actual measurement height to the new reference height of 120 cm.

The total uncertainty of an observed gravity value is composed of the gravity measurement precision σ_g, system errors σ_{SYS}, setup error σ_{SETUP}, and vertical transfer (gradient) error $\sigma_{\partial g/\partial H}$ (Niebauer et al., 1995). σ_{SYS} includes (i) instrumental errors (laser, clock, system model) and (ii) modeling errors (barometer, polar motion, Earth tide, ocean loading). Using formal error propagation and thereby assuming the error terms are uncorrelated, the total uncertainty σ_{tot} is given by

$$\sigma_{\text{tot}} = \sqrt{\sigma_g^2 + \sigma_{\text{SYS}}^2 + \sigma_{\text{SETUP}}^2 + \left(\sigma_{\partial g/\partial H} \times H_{\text{TRANS}}\right)^2}, \tag{2}$$

where H_{TRANS} is the difference between actual measurement height (top of the drop) and reference height. The measurement precision σ_g is the standard deviation of the mean of all sets, i.e., the set to set scatter σ_{SET} divided by the square root of the number of sets. We take $\sigma_{\text{SYS}} \approx 1.6$ μGal as given in g9 by the manufacturer. Instead of the $\sigma_{\text{SETUP}} = 1.0$ μGal estimate suggested in g9, however, we adopt the more conservative $\sigma_{\text{SETUP}} = 1.6$ μGal estimate of Van Camp et al. (2005).

We investigated the stability of the FG5-226 by checking for time-variable instrument offsets, trends or drift. Fig. 3 shows the gravity time series using all sufficiently long FG5-226 gravity campaigns at its home site, NMBU. The mean gravity value has been subtracted from each observation, and the observations have been corrected for GIA using a recent modeled linear rate of change in gravity, $\dot{g}_M$, as described in Section 3. We observe the remaining secular gravity trend to be 0.0 ± 0.1 μGal yr^{-1} and insignificant. A similar conclusion can be drawn from Fig. 4, which shows the gravity time series using FG5-226 observations at all gravity sites where more than one observation is available. Here, the mean gravity value of each site has been removed from GIA-corrected site observations, giving several time series which are ultimately plotted in the same figure. Again we observe an insignificant remaining gravity trend of 0.1 ± 0.4 μGal yr^{-1}. Furthermore, we do not observe any nonlinear structure in neither Fig. 3 nor Fig. 4. We therefore conclude that the FG5-226 has no significant drift, which suggests it has been stable throughout the observation span of this work.

Table 2
FG5-generation of absolute gravimeters used in Norway 1993–2014.

Instrument	Agency	Reference
FG5-226 (2004–2014)	Norwegian University of Life Sciences (NMBU), Ås, Norway	This work
FG5-233 (2007)	Lantmäteriet (LM), Gävle, Sweden	
FG5-220 (2003–2007)	Institut für Erdmessung (IfE), Leibniz Universität Hannover, Germany	(Roland, 1998)
FG5-101 (1993–1998), FG5-301 (2003)	Bundesamt für Kartographie und Geodäsie (BKG), Frankfurt, Germany	(Gitlein, 2009)
FG5-102 (1993), FG5-111 (1995, 1997)	National Oceanic and Atmospheric Administration (NOAA), Silver Spring, Maryland, USA	G. Sasagawa, personal communication, 2005

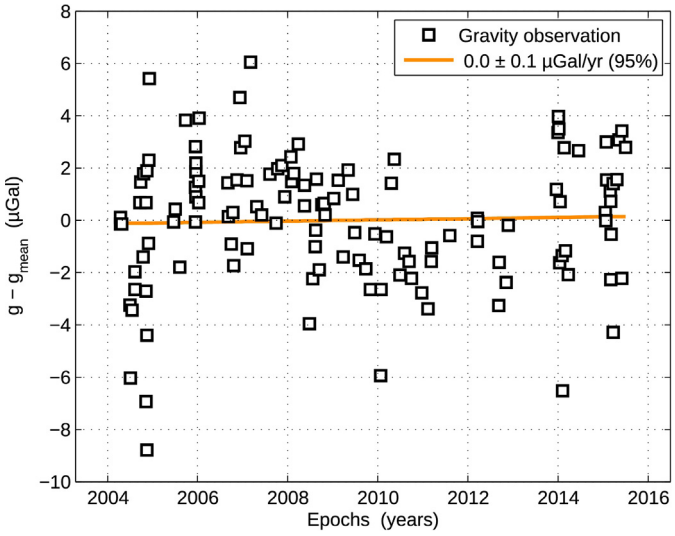

Fig. 3. Stability of the FG5-226 AG meter for the 2004–2015 period, as derived from all repeated gravity observations at NMBU. The gravity time series is reduced for the site-specific mean value and GIA trend, thus showing residual temporal variations including instrumental drift only.

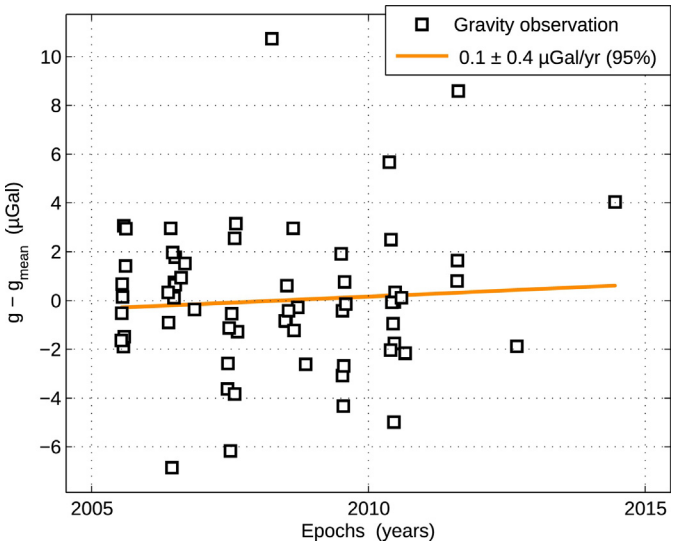

Fig. 4. Stability of the FG5-226 AG meter for the 2005–2014 period, as derived from repeated gravity observations at 20 different sites. The gravity time series of each station is reduced for the site-specific mean value and GIA trend, thus showing residual temporal variations including instrumental drift only.

Standard g9 gravity estimates g_0 and uncertainties are shown in the supplementary data Table S1.

2.1. Ocean loading effects

The majority of the AG sites in Norway are located within 2 km of the coast (see Fig. 1). It has been previously shown that these stations may be strongly influenced by ocean tide loading (OTL) (e.g., Lysaker et al., 2008; Breili, 2009; Breili et al., 2010). In addition, non-tidal variation of sea level due to low barometric pressure and strong winds may affect gravity (Olsson et al., 2009).

OTL and non-tidal loading (NTL) have different characteristics. Along the Norwegian coast, OTL may introduce deterministic semi-diurnal patterns with amplitudes of several µGal in time series of gravity (Lysaker et al., 2008). As a result, the variation of the set to set scatter of a gravity campaign may increase if appropriate OTL corrections are not applied. Furthermore, the campaign averages and derived secular trends may be biased (Timmen et al., 2015). This is particularly relevant for short campaigns not covering an integer multiple of the dominating tidal periods. NTL, on the other hand, is non-deterministic and non-periodic; hence, corrections must be computed from observations. As NTL may be close to constant during a campaign, its impact on gravity is difficult to infer from inspection of the set to set scatter alone.

In the following we investigate different OTL corrections and identify OTL models that are most successful in reducing the campaign set to set scatter (σ_{SET}).

In general, OTL corrections are easily computed from predetermined amplitude and phase coefficients for sinusoids with frequencies matching the major tidal constituents (Petit and Luzum, 2010, Ch. 7). The coefficients are computed by convolving global ocean tide (GOT) models with Green's functions formed by load Love numbers (Farrell, 1972), and are available through M.S. Bos and H.-G. Scherneck's Ocean tide loading provider at http://holt.oso.chalmers.se/loading/. This procedure is also implemented in g9, and for our standard gravity estimates (g_0, see Table S1), OTL was computed with the FES2004 GOT model (Lyard et al., 2006), with the exception of KAUT and TRYB/TRYC, where no OTL effect was computed due to their inland locations.

An important difference between g9 and the OTL provider is that the latter refines the spatial resolution of the GOT model gradually towards the observation point and checks whether new GOT cells are located on land or sea (Penna et al., 2008). g9 also refines the GOT model towards the observation point, but does no land/sea check of the new cells (O. Francis, personal communication, 2016).

With coefficients from the OTL provider we have explored a suite of GOT models, i.e., FES2004, CSR4.0 (Eanes, 1994), DTU10 (Cheng and Andersen, 2010), EOT11 (Savcenko and Bosch, 2011), GOT4.8 (Ray, 1999), NAO99b (Matsumoto et al., 2000), OSU12 (Fok et al., 2012), Schwiderski (Schwiderski, 1980), and TPXO7.2 (Egbert and Erofeeva, 2002). These models were chosen as they represent the latest release from each group available at the OTL provider.

Lysaker et al. (2008) showed that careful local modeling of the OTL correction (direct Newtonian and displacement of the observing point due to load) corresponded better with the OTL signal at selected high-latitude coastal stations in Norway than did the effect computed from GOT models. Thus for FES2012 (produced by Noveltis, Legos, and CLS Space Oceanography Division and distributed

Table 3
The gravitational and loading effects of a one-meter sea-level anomaly within 10 km of coastal gravity sites in Norway, and the amplitude of the M2 tidal constituent for the attraction component. All in μGal.

Code	Gravitation due to a 1 m sea-level anomaly	Loading due to a 1 m sea-level anomaly	Amplitude of M2 (attraction only)
ANDO	3.4	0.20	3.7
BODB	0.6	0.22	1.1
BODA	0.3	0.25	0.8
HAMM	3.1	0.13	3.0
HONN	6.4	0.28	5.9
JON2	4.8	0.16	1.5
KOL1	0.3	0.29	0.1
KOL2	0.5	0.30	0.2
STVA	1.5	0.26	0.2
TROM	1.4	0.14	1.6
TRDA	2.6	0.27	2.1
VAGA	4.2	0.21	3.2
VEGA	0.1	0.17	0.6
ALES	9.8	0.26	6.9

by Aviso, with support from CNES, at http://www.aviso.altimetry.fr) as well as NAO99b, we investigate OTL corrections as computed by an in-house software. The routines closely follow methods used by the OTL provider, although with two important distinctions.

First, we have used a higher-resolution coastline provided by the Norwegian Mapping Authority (NMA), with a level of detail corresponding to national maps in scale 1:50,000, and termed the N50 coastline hereafter. It is complete and includes all islands and reefs along the Norwegian coast with an area greater than 20,000 m^2.

Second, our software allows for choosing which regions are to be included in the convolution. We have used this functionality to investigate the effect of replacing the GOT model with predicted tides based on tide-gauge observations when computing the attraction from the tides in the local zone. The local zone is here defined as the area within 10 km of the gravity site. The method is a development of the one demonstrated by Lysaker et al. (2008). By this approach the gravitational effect of the local tides was modeled by (i) dividing the local zone into spherical sectors, (ii) assigning to each sector a uniform layer of water corresponding to sea level as observed by a local tide gauge, (iii) computing the attraction from each sector, (iv) eliminating sectors on land, and (v) add together the contributions from the individual ocean sectors.

The size of the spherical sectors was adjusted depending on the distance from the observation point, i.e., the length of the outer arc was set to 25, 50, and 200 m in the zones 0–500, 500–1000, and 1000–10,000 m from the observation point, respectively. Each sector was classified as land or ocean by comparing the sector midpoint coordinates with the N50 coastline.

In this work, NTL is the combined effect of gravitational attraction and loading of the seabed due to non-tidal variations in sea level. The gravitational attraction component was modeled by the above procedure, using spherical sectors with a water thickness equal to the difference between actual and predicted sea level as observed by a local tide gauge. For the loading components, we assumed that sea level responds like an inverted barometer (IB, static atmospheric loading effect). This implies that sea level variation due to changing atmospheric pressure does not induce any loading on the sea floor. Thus, before computing the loading effect, observed sea level was corrected for the IB effect using Wunsch and Stammer (1997, Eq. (1)).

We have computed refined OTL and NTL corrections at 14 coastal gravity sites in Norway (Table 3), with remaining sites excluded due to their inland locations. The gravitational and loading effects of a one-meter sea-level anomaly at the coastal gravity sites is shown in Table 3, where the actual gravitational effect may be found by scaling the one-meter effect with the actual sea-level anomaly.

We have used tide-gauge records from the NMA database, with a sampling rate of 10 minutes and all observations referring to present mean sea level (1996-2014 inclusive). Unfortunately, there are no tide gauges within the local zones of JON2, KOL1, KOL2, VEGA, and VAGA. For these sites, sea level was derived by applying site-specific scale factors and time delays to observations from the nearest tide gauge. The scale factors and time delays were obtained from the tide and sea-level web service of the NMA at http://www.kartverket.no/en/sehavniva/.

For each gravity site, we identify the ocean loading corrections that reduce σ_{SET} as much as possible, combining all OTL and NTL corrections. Table 4 shows the average percentage reduction in σ_{SET} for each site. We note that STVA and JON2 stand out with low reductions. For STVA, this is due to a weak OTL signal related to a M2 amphidromic point in the North Sea, giving a locally low tidal range (0.32 m between mean high and mean low tide). At JON2 the average is strongly influenced by the 2005.482 campaign, which has a low σ_{SET} of 1.2 μGal. When applied to this campaign, σ_{SET} increases for several OTL corrections, resulting in a negative reduction of σ_{SET}.

With few exceptions, the OTL corrections computed by g9 reduce σ_{SET} less than the corrections computed by the OTL provider or the in-house software. This also holds for FES2004 as used by both g9 and the OTL provider.

Table 4 suggests that N50 improves the fit between observations and models at several sites (e.g., NAO99b(N50) compared with NAO99b(OTLP), and FES2012(N50) compared with FES2004(OTLP)). Largest improvements are found at HONN and HAMM for NAO99b and FES2012, and at TRDA and VAGA for NAO99b. For these combinations, the N50 coastline reduces σ_{SET} by 7.5% to 22.5%. We expect coastline accuracy to have largest influence on gravity sites that are in immediate vicinity of the ocean. Indeed the sites showing the largest improvements are also among those closest to the ocean, e.g., HAMM and HONN (75 m).

For most stations we observe further improvement when the N50 coastline is combined with local tide-gauge observations. The change in reduced σ_{SET} ranges from −0.5% to 3.7% for NAO99b, and from 0% to 21.3% for FES2012. Both TRDA and JON2 are located inside fjords. Comparing NAO99b and FES2012 at these sites, the largest effect of introducing tide-gauge observations is seen for the latter, suggesting that FES2012 does not capture the tidal regime in these fjords.

Choosing a best-performing model is challenging, as their performance depends on the gravity site. Considering all models, NAO99b and FES2012 in combination with the N50 coastline perform best at 9 out of 14 sites.

Corrections from the OTL provider give the best results at BODA, VEGA, KOL1, JON2, and STVA, where all sites but JON2 have in common that the M2 amplitude of the attraction component is less than 1 μGal (see Table 3). This suggests that careful modeling of the local zone is important mainly at sites with a strong attraction component.

Table S1 shows the final ocean loading corrections for all coastal gravity campaigns, together with standard and refined set to set scatters and the chosen ocean loading model. As the standard gravity estimates from g9, g_0, have already been corrected for OTL (Δg^0_{OTL}), we present the change in OTL correction, i.e., $\delta g_{OTL} = \Delta g_{OTL} - \Delta g^0_{OTL}$, to ease the application of the refined OTL correction Δg_{OTL}. NTL is not treated in g9; hence, the complete correction is listed as Δg_{NTL}.

Typically, OTL and NTL contribute to a campaign gravity value by a few tenths of a μGal, although some corrections reach ∼2 μGal. The refined OTL correction ranges from −0.55 μGal (STVA 2006.855) to 1.81 μGal (ALES 2006.384), while the new NTL

Table 4
Average percentage reduction in set to set scatter (σ_{SET}) for each gravity site, obtained by applying OTL corrections from different models. Also includes NTL. Sites ordered along the coast from north to south. Only campaigns where raw data is available are included.

Code	FES2004 g[a]	FES2004 OTLP[b]	CSR4.0 OTLP	DTU10 OTLP	EOT11a OTLP	GOT4.8 OTLP	OSU12 OTLP	SCHW80 OTLP	TPXO7.2 OTLP	NAO99b OTLP	NAO99b N50[c]	TG+NAO99b N50	FES2012 N50	TG+FES2012 N50
HONN	25.5	34.4	20.9	35.6	35.7	34.1	35.2	37.8	35.0	31.8	57.3	61.0	58.7	60.9
HAMM	34.6	44.2	46.0	44.4	45.1	45.1	42.9	42.9	44.4	47.3	56.8	57.0	58.2	58.3
TROM	30.0	30.8	35.0	30.6	31.4	36.4	35.9	35.9	36.9	35.6	35.3	37.0	31.2	37.7
ANDO	53.9	62.2	55.3	62.8	63.3	62.5	63.3	58.7	62.5	63.9	63.7	64.3	62.2	63.3
BODA	36.1	39.6	34.9	39.7	39.4	38.7	39.5	39.9	38.3	39.4	38.7	38.8	39.5	39.5
BODB	45.1	50.0	47.9	50.5	50.1	50.9	50.9	50.8	49.6	51.3	51.2	51.4	50.0	50.3
VEGA	25.3	26.2	26.9	25.9	25.8	26.5	26.7	25.4	25.4	26.6	26.7	26.7	26.0	26.0
TRDA[d]	21.6	26.1	21.0	25.1	25.1	25.4	25.1	23.3	29.8	34.7	42.2	45.6	24.1	45.4
ALES	25.4	46.0	44.4	45.6	45.8	47.6	42.1	30.9	41.5	48.5	49.6	50.0	48.9	50.2
VAGA	32.4	39.3	27.9	39.0	39.4	34.1	35.1	32.6	36.4	36.4	47.0	47.5	40.7	47.3
KOL1	13.8	15.2	17.5	16.3	16.7	18.2	16.9	14.6	16.7	17.3	17.4	17.3	15.6	15.7
KOL2	32.9	40.0	37.8	39.4	40.4	39.5	40.1	33.7	40.6	42.6	43.2	43.1	41.9	42.2
JON2	9.3	3.8	3.4	3.1	4.0	16.5	10.3	12.0	19.6	18.7	14.2	15.4	−0.7	17.6
STVA	−0.2	1.0	4.8	2.0	2.5	2.4	2.5	2.1	2.7	4.1	4.7	4.2	1.6	1.8

[a] Original g9 OTL correction.
[b] OTL provider.
[c] In-house software with higher-resolution coastline.
[d] Not including the 2004.475 campaign.

correction ranges from −1.86 μGal (ALES 2003.715) to 1.04 μGal (ALES 2008.724).

2.2. Atmospheric and hydrological effects

Atmospheric density variations in time cause changes in the direct Newtonian gravitational attraction from the air mass around the gravimeter, as well as varying crustal and ocean surface deformation due to loading. Conventionally, local pressure and gravity variations are correlated with an admittance factor of $A = 0.30$ μ Gal/hPa, in accordance with IAG Resolution No. 9, 1983. This admittance factor is used in the correction Δg_{ATM} for atmospheric pressure implemented in g9, $\Delta g_{ATM} = A(P_o - P_n)$, where P_o is the in situ pressure as observed by the FG5 barometer, and $P_n = 1013.25\left(1 - 0.0065H/288.15\right)^{5.2559}$ is the nominal barometric pressure (H is the gravity site height in meters), in accordance with DIN Standard #5450. A more precise description of A allows it to vary in space and time, and depend on the total global mass distribution of the atmosphere. Typically, an improved atmospheric effect on gravity is computed by incorporating atmospheric mass attraction and load considering zones of increasing distance to the gravity site (Gitlein et al., 2013).

Having reduced the gravity value for the time-variable tidal, polar motion, and atmospheric mass components, it may remain strongly influenced by hydrological variations (Mikolaj et al., 2015). The effect of hydrology on the observed gravity value is usually not considered when processing absolute gravity observations (Timmen, 2010), and is not treated in g9.

For the computation of total atmospheric (ATM) and global hydrological (GH) effects on gravity we have tested the novel MATLAB® tool mGlobe (Mikolaj et al., 2016), developed at the German Research Centre for Geosciences (GFZ) in collaboration with the University of Vienna, obtained from https://github.com/emenems/mGlobe (M. Mikolaj, personal communication, 2015).

For the computation of the ATM effect, we have used 2D and 3D European Centre for Medium-Range Weather Forecasts (ECMWF) Interim Reanalysis (ERA Interim) data (Dee et al., 2011) as input model, obtained from http://apps.ecmwf.int/datasets/data/interim-full-daily. The temporal resolution was chosen to be six-hourly, and all data are given on 0.75°×0.75° grids, with a surface geopotential (orography) grid as height reference (where the height in meters is obtained by dividing the geopotential with 9.80665 ms^{-2}).

Using the coarse orography resolution of 0.75°×0.75° will often give large height discrepancies between actual gravity site height and orography height. This spatial deficiency, together with temporal deficiency (six-hourly), can be taken into account by considering the difference between pressure data from ERA Interim at orography height and actual in situ pressure at gravity site height. This difference in ATM effect, or residual effect ϵ, is then computed by the single admittance approach outlined in the above, i.e.,

$$\epsilon = -A\left(P^{\text{site}}_{\text{in situ}} - P^{\text{oro}}_{\text{ERA}}\right), \tag{3}$$

where A is the site-specific admittance factor. Gitlein (2009) estimated A at ANDO, BODB/BODA, HONN, KAUT, TROM, TRDA, TRYB/TRYC, ALES, and NMBU as well as a mean value of 0.32 μGal/hPa for Fennoscandia using ECMWF data. For the computation of Eq. (3) we used the site-specific A where available, and the mean value for Fennoscandia for the remaining sites.

We do not have actual in situ pressure measured by the FG5 barometer for the adopted gravity values (where we do not have raw data). Therefore, we obtained in situ pressure data for all gravity campaigns by cubic spline interpolation of six-hourly pressure data from nearby meteorological stations of the eKlima database of the Norwegian Meteorological Institute at http://eklima.met.no. The average distance between the meteorological station and the gravity site is ∼23 km.

We investigated the applicability of the interpolated in situ pressure values by comparing them with actual in situ pressure measured by the FG5 barometer where available (86 campaigns). Simulated single admittance ATM corrections were computed using interpolated in situ pressure and compared with those from g9. The mean difference between simulated and actual ATM correction is ∼0.4 μGal. In addition, we checked the pressure values of ERA Interim against the interpolated pressure values (for the same 86 campaigns and with ERA and eKlima pressure at equal height), and found a mean difference of ∼0.7 hPa, in agreement with previous comparisons of in situ and ECMWF pressure (Gitlein, 2009). We therefore conclude that the interpolated in situ pressure values are applicable.

For the computation of the GH effect, we have used the ACE2 30” × 30” digital elevation model (DEM) (Berry et al., 2010), as well as the Global Land Data Assimilation System (GLDAS) Version 2 NOAH (0.25°×0.25°) hydrological data (Rodell et al., 2004), downloaded through mGlobe. GLDAS has two versions, 2.0 and 2.1, covering the time periods 1948–2010 and 2000–2015, respectively. Where available, we have used the most recent

version. GLDAS/NOAH captures the contribution of global continental water storage to gravity variations by considering four soil moisture layers (0–10 cm 10–40 cm, 40–100 cm, and 100–200 cm) and snow (snow water equivalent); hence, it does not consider groundwater.

Although the IAG resolution (1983) recommends the removal of the mean atmosphere, this is not done in the current version of mGlobe, which computes effects with respect to an arbitrary reference (M. Mikolaj, personal communication, 2015). However, an absolute reference is not important here as we only consider temporal variations. Thus, we have computed long-term means of both ATM ($\bar{g}^{\mathrm{ERA}}_{\mathrm{ATM}}$) and GH ($\bar{g}^{\mathrm{GLDAS/NOAH}}_{\mathrm{GH}}$) effects and subtracted these from the short-term effects $g^{\mathrm{ERA}}_{\mathrm{ATM}}$ and $g^{\mathrm{GLDAS/NOAH}}_{\mathrm{GH}}$. For consistency, we have chosen the time period 2004-2009 inclusive for both mean ATM and GH effects. Fig. 5 shows the variation of mean ATM and GH effects at NMBU for the chosen epoch. The mean value at a given time step is computed using mGlobe output up to this time step only, i.e., it is computed in a cumulative fashion. We observe that the variation of the mean ATM effect stabilizes earlier than the mean GH effect, and by the end of the sixth year, both means vary by less than ~0.03 μGal, which is well within model uncertainties. Thus, we conclude that the chosen time period suffices as a stable long-term mean for all gravity sites in this work. Short-term ATM and GH effects were computed using six-hourly and daily resolutions, respectively, overlapping the gravity campaigns. For the ATM effect, overlapping values were subsequently interpolated to the actual time spans of the gravity campaigns.

The correction for the GH effect was computed according to

$$\Delta g_{\mathrm{GH}} = -\left(g^{\mathrm{GLDAS/NOAH}}_{\mathrm{GH}} - \bar{g}^{\mathrm{GLDAS/NOAH}}_{\mathrm{GH}}\right). \tag{4}$$

Computing the ATM correction is slightly more laborious. First, the 2004–2009 long-term mean $\bar{\epsilon}$ of the residual effect (Eq. (3)), was computed. Second, there will be a bias β between the ATM correction referring to the long-term mean pressure using ERA Interim, $\bar{P}^{04-09}_{\mathrm{ERA}}$, and the standard ATM correction referring to nominal pressure P_n. To ease comparison and facilitate the computation of the difference between standard and refined corrections, we computed β at orography height according to

$$\beta = 0.3\left(P_n - \bar{P}^{04-09}_{\mathrm{ERA}}\right). \tag{5}$$

Finally, the correction for the ATM effect was computed by

$$\Delta g_{\mathrm{ATM}} = -\left[\left(g^{\mathrm{ERA}}_{\mathrm{ATM}} - \bar{g}^{\mathrm{ERA}}_{\mathrm{ATM}}\right) + \left(\epsilon - \bar{\epsilon}\right) + \beta\right]. \tag{6}$$

Table S1 shows ATM and GH corrections for all gravity campaigns. As was the case for ocean loading, the standard gravity estimates from g9, g_0, have already been corrected for the ATM effect ($\Delta g^0_{\mathrm{ATM}}$), and we present the change in ATM correction, i.e., $\delta g_{\mathrm{ATM}} = \Delta g_{\mathrm{ATM}} - \Delta g^0_{\mathrm{ATM}}$. Hydrology is not treated in g9; hence, we list the complete correction Δg_{GH}.

The refined ATM correction ranges from −1.9 μGal (TRYC 2003.723) to 1.1 μGal (e.g., HONN 2007.507), which is in the same order as the refined ATM corrections of Gitlein (2009). The GH correction ranges from −1.5 μGal (TRYB 2008.254) to 1.7 μGal (TRYC 2006.614), corresponding to previous studies (e.g., Pálinkáš et al., 2012; Mikolaj et al., 2015).

3. Secular gravity trends and gravity-to-height ratios

Table 5 shows secular gravity trends for each observation site. The rates $\dot{g}_0$ and $\dot{g}$ were computed by fitting a linear trend using ordinary least-squares regression (OLR, without weights) to the gravity data sets g_0 and g of Table S1, respectively. The percentage change $\Delta_{\dot{g}}$ of $\dot{g}$ with respect to $\dot{g}_0$ has been computed, as well as statistics (for sites with more than two observations) in the form of coefficients of determination for both $\dot{g}_0$ and $\dot{g}$, and the 95% confidence interval for $\dot{g}$. The coefficient of determination was computed according to $R^2 = 1 - SSR/SST \in [0, 1]$, where SSR and SST are the residual and total sum of squares, respectively.

R^2 indicates how well the linear model fits the gravity data, and will increase as the model fit to the data improves. R^2_0 and R^2 denote the coefficient of determination for the standard gravity estimates g_0 and the refined estimates g, respectively. Looking at Table 5, we note that both R^2_0 and R^2 reveal both good and bad linear model fits. R^2 gives a better fit to the linear model than R^2_0 at nine sites. 95% confidence intervals shows a significantly negative trend at six sites.

In order to assess our empirical gravity rates, a modeled gravity rate, $\dot{g}_M$, was computed using height rates of change $\dot{h}$ from a recent empirical absolute land uplift model (given in ITRF2008) of the NMA, based on a combination of GNSS and leveling (O. Vestøl, personal communication, 2015), together with a recent modeled relation between gravity and height rates of change $\left(\dot{g}/\dot{h}\right)_M$ of $-0.163\ \mu\mathrm{Gal\,mm^{-1}}$ for GIA (Olsson et al., 2015) (Table 5). It is generally challenging to quantify the uncertainty of $\left(\dot{g}/\dot{h}\right)_M$, as it incorporates uncertainties of both the ice and Earth models used. However, Olsson et al. (2015) computed $\left(\dot{g}/\dot{h}\right)_M$ for Fennoscandia using six Earth models with varying upper mantle viscosities (their Table 3), giving a maximum difference of $0.008\ \mu\mathrm{Gal\,mm^{-1}}$. We adopted this model spread multiplied by two as an uncertainty estimate for $\left(\dot{g}/\dot{h}\right)_M$, yielding $0.016\ \mu\mathrm{Gal\,mm^{-1}}$ (H. Steffen, personal communication, 2016). The uncertainties of $\dot{h}$ were determined as a sum of the observation error and systematic errors due to origin drift along the three directions ($0.5\ \mathrm{mm\,yr^{-1}}$) and scale error ($0.3\ \mathrm{mm\,yr^{-1}}$) of the reference frame (Collilieux et al., 2014). In turn, the uncertainties of $\dot{g}_M$ were computed by formal error propagation.

Considering $\dot{g}_M$ as a "true" reference, $\Delta_{\dot{g}}$ indicates that $\dot{g}$ performs better than $\dot{g}_0$ at nine gravity sites. For the remaining sites, the refined gravity corrections give no significant improvement or even degrade the trend. We note that these results are similar to the results of Gitlein (2009), where refined ATM corrections were estimated and found to improve the gravity rates at 6 out of 11 sites, with no observed improvement on average. We also note that in some cases, although the linear model fit degrades, the rate itself is improved.

Similar conclusions can be drawn from Fig. 6, which shows the linear gravity rates $\dot{g}_0$, $\dot{g}$, and $\dot{g}_M$ for all gravity sites. With the exception of HONC and TROM, the observed gravity rates are larger than the modeled ones, particularly BODA, KAUT, and TRDA.

Combining linear rates of change in gravity and height gives a convenient means for interpreting the physical processes underlying vertical crustal deformation, and is the only way to distinguish a gravity change due to vertical deformation from gravity change due to mass redistribution (de Linage et al., 2007). The relation between gravity and height rates of change due to GIA in Fennoscandia has been subject to extensive research, and the proportionality constant between gravity and height rates of change determined within the range of -0.154 to $-0.217\ \mu\mathrm{Gal\,mm^{-1}}$ (e.g.,Wahr et al., 1995; Ekman and Mäkinen, 1996; Gitlein, 2009; Pettersen, 2011; Olsson et al., 2015).

Based on the results presented in Fig. 6, we formed a subset of reliable rates, where a reliable rate is defined as within the uncertainty of $\dot{g}_M$. In other words, an agreement of $\dot{g}_0$ or $\dot{g}$ with $\dot{g}_M$ gives us confidence in that the empirical rates mainly reflect GIA. The subset contains empirical gravity rates from 10 sites, namely BODB, HONN, HONA, HONB, KOL1, STVA, TRYB, TRYC, ALES, and NMBU. These rates have been used for the following comparison of gravity and height rates of change.

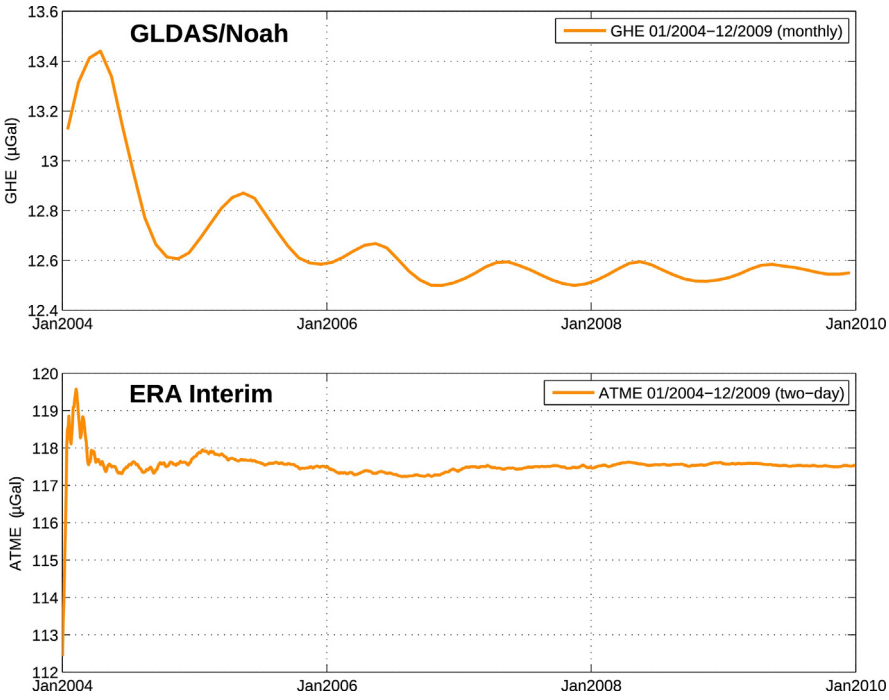

Fig. 5. Variation of mean ATM and GH effect at NMBU 2004–2009, as computed with mGlobe. The mean value at a given time step is computed cumulatively, using mGlobe output up to this time step only.

Fig. 6 and Table 5 reveal a considerable variation in the uncertainties of the empirical gravity rates, suggesting a weighted linear regression (WLR) approach for the estimation of gravity versus height rates of change. It is not possible to derive uncertainties for the gravity rates at HONA and KOL1, as they are based on two observations only. We approximated these uncertainties by plugging an average of both campaign uncertainties ($\overline{\sigma}_{\text{tot}}$) as well as their time span into Eq. (1). This gives uncertainties of $\sigma_{\dot{g}} \approx 0.5\,\mu\text{Gal yr}^{-1}$ and $\sigma_{\dot{g}} \approx 1.7\,\mu\text{Gal yr}^{-1}$ for HONA and KOL1, respectively. Eq. (1) must be taken as a rough uncertainty estimate when only two observations are used, and we consider the uncertainty estimate of KOL1 unrealistically large. Therefore, we decided to use both OLR and WLR approaches.

Fig. 7 shows gravity versus height rates of change using the standard gravity rates $\dot{g}_0$, which yields a WLR of $\dot{g}_0 = -0.135\,(\pm 0.100) - 0.142\dot{h}\,(\pm 0.018)\,\mu\text{Gal yr}^{-1}$ and an OLR of $\dot{g}_0 = -0.175\,(\pm 0.137) - 0.143\dot{h}\,(\pm 0.032)\,\mu\text{Gal yr}^{-1}$. Using $\dot{g}$, Fig. 8 shows a WLR of $\dot{g} = -0.210\,(\pm 0.183) - 0.133\dot{h}\,(\pm 0.030)\,\mu\text{Gal yr}^{-1}$ and an OLR of $\dot{g} = -0.097\,(\pm 0.196) - 0.167\dot{h}\,(\pm 0.045)\,\mu\text{Gal yr}^{-1}$. We first note that WLR and OLR based on $\dot{g}_0$ are quite similar, while WLR and OLR based on $\dot{g}$ differ considerably. Considering the constant terms and their relatively large uncertainties, only OLR based on $\dot{g}$ is statistically equal to zero. The regression slopes based on OLR ($\left(\dot{g}/\dot{h}\right)_0 = -0.143\,(\pm 0.032)\,\mu\text{Gal mm}^{-1}$, $\left(\dot{g}/\dot{h}\right) = -0.167(\pm 0.045)\,\mu\text{Gal mm}^{-1}$) and WLR ($\left(\dot{g}/\dot{h}\right)_0 = -0.142\,(\pm 0.018)\,\mu\text{Gal mm}^{-1}$, $\left(\dot{g}/\dot{h}\right) = -0.133\,(\pm 0.030)\,\mu\text{Gal mm}^{-1}$) are all in

Table 5
Linear rates of change in gravity and height.

Code	$\dot{g}_0$ (μGal yr^{-1})	R_0^2	$\dot{g}$ (μGal yr^{-1})	R^2	CI$_{\dot{g}}$ [L U][a] (μGal yr^{-1})	$\dot{g}_M$ (μGal yr^{-1})	$\Delta_{\dot{g}}$[b] (%)	$\dot{h}$[c] (mm yr^{-1})
ANDO	-1.13 ± 0.38	74.2	-0.91 ± 0.44	58.7	[−2.32 0.49]	-0.24 ± 0.11	19.5	1.47 ± 0.63
BODB	-1.06 ± 0.63	59.0	-1.18 ± 0.62	64.4	[−3.46 1.49]	-0.55 ± 0.12	−11.0	3.35 ± 0.62
BODA	-2.28 ± 0.39	94.6	-2.31 ± 0.44	93.3	[−4.19 −0.43]	-0.54 ± 0.12	1.4	3.33 ± 0.62
HAMM	−1.44		−1.61			-0.37 ± 0.11	11.9	2.26 ± 0.66
HONN	-0.38 ± 1.04	4.2	-0.57 ± 0.57	24.7	[−2.39 1.26]	-0.31 ± 0.11	−49.9	1.93 ± 0.67
HONA	−0.82		−0.88			-0.82 ± 0.13	−7.3	5.04 ± 0.62
HONB	-0.93 ± 0.09	98.2	-1.02 ± 0.13	96.8	[−1.58 −0.45]	-0.83 ± 0.13	−9.4	5.09 ± 0.62
HONC	-0.15 ± 0.27	2.9	-0.24 ± 0.27	7.3	[−0.84 0.36]	-0.82 ± 0.13	−62.8	5.01 ± 0.62
JON2	−0.80		−0.65			-0.33 ± 0.11	19.1	2.03 ± 0.61
KAUT	-2.16 ± 0.38	91.7	-2.43 ± 0.39	92.6	[−3.68 −1.17]	-0.79 ± 0.13	−12.2	4.84 ± 0.63
KOL1	−0.38		−0.12			-0.25 ± 0.11	67.8	1.54 ± 0.63
KOL2	−0.93		−0.75			-0.25 ± 0.11	19.7	1.54 ± 0.63
STVA	-0.42 ± 0.24	37.6	-0.53 ± 0.23	50.7	[−1.13 0.07]	-0.22 ± 0.10	−27.6	1.32 ± 0.61
TROM	-0.08 ± 0.19	2.8	-0.12 ± 0.18	6.3	[−0.57 0.33]	-0.42 ± 0.11	−50.0	2.59 ± 0.62
TRDA	-1.84 ± 0.24	87.9	-1.82 ± 0.22	89.3	[−2.33 −1.31]	-0.70 ± 0.12	1.1	4.28 ± 0.61
TRYB	-1.32 ± 0.27	82.4	-1.39 ± 0.24	87.2	[−2.01 −0.78]	-1.10 ± 0.15	−4.8	6.74 ± 0.62
TRYC	-1.05 ± 0.08	91.5	-1.06 ± 0.07	93.3	[−1.22 −0.90]	-1.10 ± 0.15	−1.0	6.74 ± 0.62
VAGA	-0.86 ± 0.11	96.7	-0.81 ± 0.22	86.6	[−1.77 0.16]	-0.33 ± 0.11	5.7	2.03 ± 0.61
ALES	-0.29 ± 0.14	60.7	-0.01 ± 0.31	0.0	[−0.99 0.97]	-0.26 ± 0.10	96.3	1.60 ± 0.62
NMBU	-0.55 ± 0.24	39.1	-0.58 ± 0.29	33.1	[−1.26 0.09]	-0.77 ± 0.13	−5.5	4.74 ± 0.61

[a] Lower (L) and upper (U) limits of the 95% confidence interval for $\dot{g}$.
[b] Change of $\dot{g}$ with respect to $\dot{g}_0$.
[c] From the NMA empirical land uplift model, given in ITRF2008.

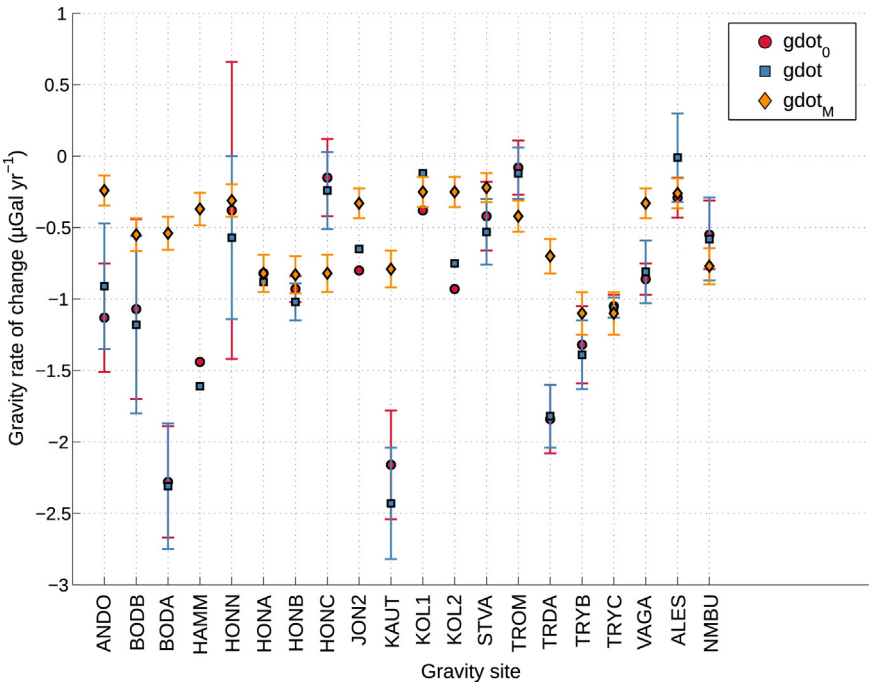

Fig. 6. Linear rates of change in gravity. $\dot{g}_0$ and $\dot{g}$ are empirical linear gravity rates based on standard and refined gravity corrections, respectively. $\dot{g}_M$ are modeled rates using a recent empirical land uplift model together with a theoretical relation between the gravity and height rate of change for GIA.

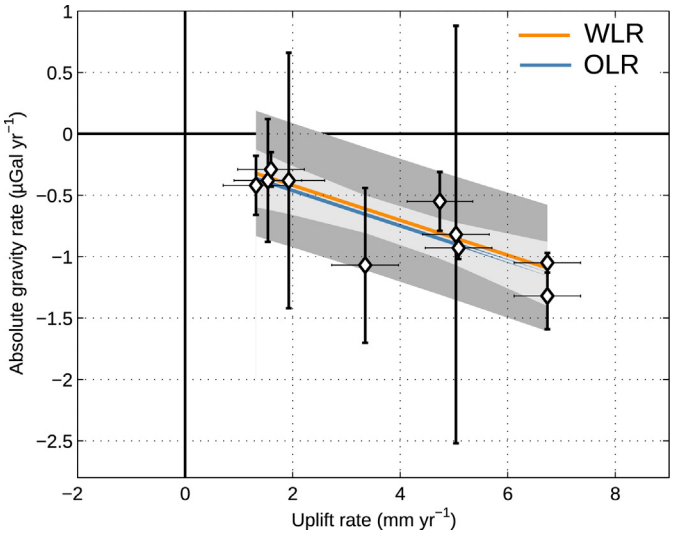

Fig. 7. Gravity versus height rates of change based on standard gravity rates $\dot{g}_0$. Height rates given in ITRF2008. The white diamonds denote the gravity site, with vertical (gravity) and horizontal (height) error bars reflecting the respective uncertainties. The solid orange line shows the WLR, with the dark gray area showing its 95% confidence interval. The solid blue line shows the OLR, with the light gray area showing its 95% confidence interval. (For interpretation of the references to colour in this figure legend, the reader is referred to the web version of this article.)

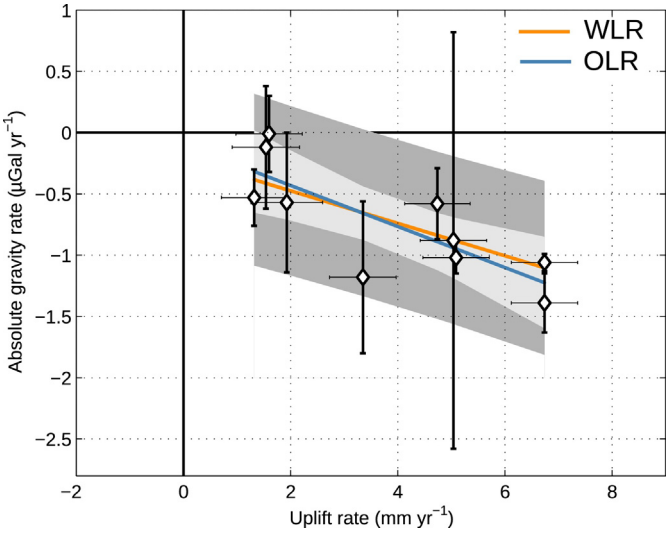

Fig. 8. Same as Fig. 7, but based on refined gravity rates $\dot{g}$.

agreement with $\left(\dot{g}/\dot{h}\right)_M$ and the reported range. However, in general, $\dot{g}$ gives a more uncertain regression than $\dot{g}_0$.

4. Discussion

There are limitations in our refined modeling of ATM and GH gravitational effects. We expect an ATM modeling inaccuracy due to using the coarse orography rather than a DEM in the local zone. In turn, the residual effect needs in-situ pressure observations which were not available for all campaigns, further limiting the accuracy. For the GH effect, an obvious limitation is that the local zone is completely left out, when it is predominantely the local hydrology in the local zone which is expected to impact on the observations (e.g., Virtanen et al., 2006; Leirião et al., 2009). Further, as GLDAS/NOAH explicitly does not include the effect of groundwater variations, these have not been considered neither globally nor locally. Groundwater variations may lead to gravity changes in the order of ∼6–7 μGal depending on local topography and ground porosity (Breili and Pettersen, 2009), and may dominate our considered effects.

Regressions based on two gravity campaigns only, i.e., HAMM, HONA, JON2, KOL1 and KOL2 are inherently uncertain, and although HONA and KOL1 present reasonable trends, they are obviously not in agreement with the needed number of observations as prescribed by Eq. (1). Because of the larger gravity rate uncertainties at HONA and KOL1, the WLR is similar to a linear regression where

both are left out. Thus, the WLR underlines the difficulty of using these rates.

Fig. 1 shows that the majority of the Norwegian AG sites are located along the coast, relatively close to the zero-line of present GIA-induced rebound in Fennoscandia. Consequently, at these sites, the signal we aim to describe (GIA) is weak, and other site-specific unmodeled processes or observation noise may dominate the rates.

Although the main component of vertical land movement in Fennoscandia is GIA, smaller elastic processes (present-day changes due to, e.g., local tectonics or melting glaciers) may also give rise to vertical deformations. For example, by observing a misfit between observed uplift (using tide gauges, leveling, GPS, and gravity) and a GIA model, Fjeldskaar et al. (2000) found a weak tectonic uplift in the order of $\sim$1 mm yr^{-1} in addition to the uplift due to GIA in large parts of Norway. Other results confirm this misfit between GIA model and observations in the Norwegian area between 65°N and 68°N (e.g., Olesen et al., 2013; Kierulf et al., 2014), suggesting that this area might not be primarily affected by GIA, but other geophysical processes. Therefore, the Norwegian data set alone is insufficient for extensive GIA modeling in Fennoscandia, a topic which is left to the NKG joint analysis on postglacial gravity change, considering observations in the entire region.

Bearing the above considerations in mind, we return to our assessment of the refined gravitational corrections (Section 3). Here we consider a reliable secular gravity trend as one in agreement with $\dot{g}_M$, i.e., a GIA model. Thus, if the rate at a gravity site agrees well with $\dot{g}_M$ it is reasonable to believe that the vertical displacement of that site is dominated by GIA. For almost all gravity rates of the reliable subset chosen in Section 3, $\dot{g}_0$ agrees more with $\dot{g}_M$ than does $\dot{g}$. In other words, the refined gravitational corrections do not offer an improvement of the reliable rates, which might be expected, as the refined corrections mainly impact gravity sites that are not dominated by GIA. At sites that are still affected by residual signals caused by other geophysical processes than GIA, refined and additional modeling is needed. Exceptions are TRYC and NMBU; however, at these sites $\dot{g}_0$ and $\dot{g}$ are quite similar.

Consequently, $\dot{g}_M$ might not be the optimal choice for assessing the refined corrections, as an agreement with $\dot{g}_M$ occurs at sites where GIA already is the dominant signal. At sites where $\dot{g}$ and $\dot{g}_0$ depart from $\dot{g}_M$ (e.g., ANDO, BODA, HAMM, KAUT, and TRDA), the signal is possibly dominated by other processes (e.g., tectonics, groundwater). Heck and Mälzer (1983) investigate $\left(\dot{g}/\dot{h}\right)$ for tectonic processes using leveled heights and relative gravimetry, giving a linear regression of ~ -1.5 μGal mm^{-1}. Thus, if we consider a tectonic uplift of $\sim$1 mm yr^{-1}, the resulting gravity change could be $1-2$ μGal yr^{-1}. Furthermore, de Linage et al. (2009) explore the variability of $\left(\dot{g}/\dot{h}\right)$ due to different surface loads, and report that $\left(\dot{g}/\dot{h}\right)$ is quite sensitive to local masses, where smaller surface load sizes give larger absolute values of $\left(\dot{g}/\dot{h}\right)$. For example, they give a mean ratio of ~ -0.87 μGal mm^{-1} over continents due to hydrological loading.

We stress, however, that it remains to be verified whether the observed deviations from $\dot{g}_M$ are due to the geophysical processes discussed herein. In addition to other geophysical processes, the misfit between GIA model and observations may be explained by errors in the GIA model or observation errors (GNSS, leveling, and AG).

The stability and accuracy of AG meters are usually assessed by AG intercomparisons, which have shown systematic biases between different instruments. Pettersen et al. (2010) computed gravity differences for two instruments measuring simultaneously at a site using a suite of gravimeters used in Fennoscandia 2003–2006, and obtained an rms error of ±3 μGal. The European Comparison of Absolute Gravimeters (ECAG) in 2007 (Francis et al., 2010) showed an agreement of ±2 μGal between 20 instruments, while ECAG 2011 showed an agreement of ±3.1 μGal between 22 instruments (Francis et al., 2013). The first North American comparison of 9 gravimeters showed an agreement of ±1.6 μGal (Schmerge et al., 2012). While differences that are larger than the observation uncertainties may indicate a possible systematic error, it is uncertain to which extent these differences are reproducible or stable in time. Consequently we did not consider applying an instrumental offset to our data set.

5. Conclusions

We have compiled and analyzed all Norwegian FG5 AG observations from the 1993–2014 period, with an aim of exploring the applicability of these data for GIA studies. Raw observations have been reprocessed using a common scheme, ensuring consistency with respect to model and setup parameters. Adopted observations by other instruments or agencies have been carefully incorporated in the data set, with updated uncertainties.

To improve the separation of the different gravity rate signal contributors, we have investigated whether it is possible to improve the corrections for geophysical processes other than GIA. Using a suite of GOT models, we have compared standard OTL corrections with results from a web service and an in-house software incorporating the higher-resolution coastline N50 as well as tide-gauge observations. Furthermore, we have tested the novel mGlobe tool for the computation of ATM and GH effects. Refined OTL, NTL, ATM, and GH corrections have all been applied to the standard gravity values to form refined gravity values.

Secular gravity trends based on both standard and refined corrections have been computed. These, in turn, have been compared with modeled rates based on a recent empirical land uplift model and theoretical relation between the gravity and height rate of change for GIA. The refined gravity rates mainly impact sites where GIA is not the dominant signal. This suggests that a refined modeling is meaningful at sites that are still affected by various unmodeled or insufficiently modeled effects. Compared to the modeled gravity rates, the refined gravity rates agree better than standard rates at 9 out of 20 sites. This reveals the need for further improvement of the refined corrections as well as the consideration of remaining unmodeled effects. We have not considered the effect of local hydrology in this work. Although seasonal variations will have less of an impact on the rates with time, we conclude it should be taken into account if possible (e.g., by monitoring groundwater variations).

Based on a subset of gravity trends mainly reflecting GIA, we have computed empirical estimates of the ratio between gravity and height rates of change using both standard and refined gravity corrections. The WLR gives $\dot{g}_0 = -0.135\,(\pm 0.100) - 0.142\dot{h}\,(\pm 0.018)$ μGal yr^{-1} and $\dot{g} = -0.210\,(\pm 0.183) - 0.133\dot{h}\,(\pm 0.030)$ μGal yr^{-1}, respectively. The OLR gives $\dot{g}_0 = -0.175\,(\pm 0.137) - 0.143\dot{h}\,(\pm 0.032)$ μGal yr^{-1} and $\dot{g} = -0.097\,(\pm 0.196) - 0.167\dot{h}\,(\pm 0.045)$ μGal yr^{-1}, respectively. The regression slopes are within $-0.133\,(\pm 0.030)$ to $-0.167\,(\pm 0.045)$ μGal mm^{-1}, in agreement with previous empirical and theoretical estimates. Therefore, this subset of the Norwegian data may well be embedded in the planned NKG joint analysis on postglacial gravity change, which will consider data from the entire region. We expect the subset to be augmented with additional sites in the future, as they become suitable for GIA studies through improved corrections for remaining geophysical effects and/or additional observations.

Finally, the WLR reveals the challenge of incorporating gravity rates that are based on few observations, emphasizing the need for extending the gravity time series. Both past and future observation of the AG reference frame in Norway is dependent on funding

and operator availability. Consequently, the sampling interval and number of observations at each gravity site is variable. Some of the longer time series rely on quite few observations. We therefore conclude that although the Norwegian AG data set should be applicable for further studies, extending the observation time series is decisive for improving the gravity rates, and is expected to reveal new and beneficial information at all gravity sites.

Acknowledgements

We would like to thank Andreas Engfeldt, Are Jo Næss, Per-Anders Olsson, and Glenn Sasagawa for contributions to Norwegian AG campaigns 1997–2010. Olav Vestøl at the NMA provided land uplift data. The open data policies of ECMWF and MET Norway are acknowledged, as well as NMA, BKG, IfE, and NOAA for having coordinated and made AG observations in Norway 1993–2007. Observation sites in this work are maintained and provided by Andøya Space Center, the Geological Survey of Norway, Gravitude AS, NMA, NMBU, and Statoil ASA. Finally, we are grateful for the constructive comments of the Editor and two anonymous reviewers that considerably improved the manuscript.

Appendix A. Supplementary data

Supplementary data associated with this article can be found, in the online version, at http://dx.doi.org/10.1016/j.jog.2016.09.001.

References

Arneitz, P., Meurers, B., Ruess, D., Ullrich, C., Abermann, J., Kuhn, M., 2013. Gravity effect of glacial ablation in the Eastern Alps – observation and modeling. Cryosphere 7, 491–498.

Berry, P.A.M., Smith, R.G., Benveniste, J., 2010. ACE2: the new global digital elevation model. In: Mertikas, S.P. (Ed.), Gravity, Geoid and Earth Observation, International Association of Geodesy Symposia 135. Springer, Berlin, pp. 231–237.

Breili, K., Pettersen, B.R., 2009. Effects of surface snow cover on gravimetric observations. J. Geodyn. 48, 16–22.

Breili, K., Rolstad, C., 2009. Ground-based gravimetry for measuring small spatial-scale mass changes on glaciers. Ann. Glaciol. 50, 141–147.

Breili, K., Gjevestad, J.G., Lysaker, D.I., Omang, O.C.D., Pettersen, B.R., 2010. Absolute gravity values in Norway. Norsk Geografisk Tidsskrift 64, 79–84.

Breili, K., 2009. Ocean tide loading at elevated coastal gravity stations. Kart og Plan 69, 151–164.

Cheng, Y., Andersen, O.B., 2010. Improvement in global ocean tide model in shallow water regions. In: Poster Presented at the Ocean Surface Topography Science Team Meeting, Lisbon, October 18–22.

Collilieux, X., Altamimi, Z., Argus, D.F., Boucher, C., Dermanis, A., Haines, B.J., Herring, T.A., Kreemer, C.W., Lemoine, F.G., Ma, C., MacMillan, D.S., Mäkinen, J., Métivier, L., Ries, J., Teferle, F.N., Wu, X.,2014. Ch. External Evaluation of the Terrestrial Reference Frame: Report of the Task Force of the IAG Sub-commission 1.2. In: Earth on the Edge: Science for a Sustainable Planet: Proceedings of the IAG General Assembly, Melbourne, Australia, June 28-July 2, 2011. Springer, Berlin, Heidelberg, pp. 197–202.

de Linage, C., Hinderer, J., Rogister, Y., 2007. A search for the ratio between gravity variation and vertical displacement due to a surface load. Geophys. J. Int. 171 (3), 986–994.

de Linage, C., Hinderer, J., Boy, J.-P., 2009. Variability of the gravity-to-height ratio due to surface loads. Pure Appl. Geophys. 166, 1217–1245.

Dee, D.P., Uppala, S.M., Simmons, A.J., Berrisford, P., Poli, P., Kobayashi, S., Andrae, U., Balmaseda, M.A., Balsamo, G., Bauer, P., Bechtold, P., Beljaars, A.C.M., van de Berg, L., Bidlot, J., Bormann, N., Delsol, C., Dragani, R., Fuentes, M., Geer, A.J., Haimberger, L., Healy, S.B., Hersbach, H., Hólm, E.V., Isaksen, L., Kållberg, P., Khler, M., Matricardi, M., McNally, A.P., Monge-Sanz, B.M., Morcrette, J.-J., Park, B.-K., Peubey, C., de Rosnay, P., Tavolato, C., Thpaut, J.-N., Vitart, F., 2011. The ERA-Interim reanalysis: configuration and performance of the data assimilation system. Quart. J. R. Met. Soc. 137 (656), 553–597.

Eanes, R.J., 1994. Diurnal and semidiurnal tides from TOPEX/POSEIDON altimetry (abstract). Eos Trans. AGU 75, 16. In: Spring Meeting Suppl, p. 108.

Egbert, G.D., Erofeeva, S.Y., 2002. Efficient inverse modeling of barotropic ocean tides. J. Atmos. Oceanic Technol. 19 (2), 183–204.

Ekman, M., Mäkinen, J., 1996. Recent postglacial rebound, gravity change and mantle flow in Fennoscandia. Geophys. J. Int. 126 (1), 229–234.

Farrell, W.E., 1972. Deformation of the Earth by surface loads. Rev. Geophys. 10 (3), 761–797.

Fjeldskaar, W., Lindholm, C., Dehls, J.F., Fjeldskaar, I., 2000. Postglacial uplift, neotectonics and seismicity in Fennoscandia. Quat. Sci. Rev. 19 (14–15), 1413–1422.

Fok, H.S., Shum, C.K., Yi, Y., Iz, H.B., Matsumoto, K., 2012. Improved coastal ocean tide modeling using satellite altimetry. In: Poster Presented at the 20 Years of Progress in Radar Altimetry Symposium, Venice, September 24–29.

Francis, O., Dam, T., Germak, A., Amalvict, M., Bayer, R., Bilker-Koivula, M., Calvo, M., D'Agostino, G.-C., Dell'Acqua, T., Engfeldt, A., Faccia, R., Falk, R., Gitlein, O., Fernandez, M., Gjevestad, J., Hinderer, J., Jones, D., Kostelecky, J., Le Moigne, N., Luck, B., Mäkinen, J., Mclaughlin, D., Olszak, T., Olsson, P.-A., Pachuta, A., Palinkas, V., Pettersen, B., Pujol, R., Prutkin, I., Quagliotti, D., Reudink, R., Rothleitner, C., Ruess, D., Shen, C., Smith, V., Svitlov, S., Timmen, L., Ulrich, C., Van Camp, M., Walo, J., Wang, L., Wilmes, H., Xing, L.,2010. Results of the European Comparison of Absolute Gravimeters in Walferdange (Luxembourg) of November. In: Gravity, Geoid and Earth Observation: IAG Commission 2: Gravity Field, Chania, Crete, Greece, 23–27 June 2008. Springer, Berlin, Heidelberg, pp. 31–35.

Francis, O., Baumann, H., Volarik, T., Rothleitner, C., Klein, G., Seil, M., Dando, N., Tracey, R., Ullrich, C., Castelein, S., Hua, H., Kang, W., Chongyang, S., Songbo, X., Hongbo, T., Zhengyuan, L., Plinks, V., Kostelecký, J., Mäkinen, J., Näränen, J., Merlet, S., Farah, T., Guerlin, C., Santos, F.P.D., Moigne, N.L., Champollion, C., Deville, S., Timmen, L., Falk, R., Wilmes, H., Iacovone, D., Baccaro, F., Germak, A., Biolcati, E., Krynski, J., Sekowski, M., Olszak, T., Pachuta, A., Agren, J., Engfeldt, A., Reudink, R., Inacio, P., McLaughlin, D., Shannon, G., Eckl, M., Wilkins, T., van Westrum, D., Billson, R., 2013. The European Comparison of Absolute Gravimeters 2011 (ECAG-2011) in Walferdange, Luxembourg: results and recommendations. Metrologia 50 (3), 257–268.

Gitlein, O., Timmen, L., Müller, J., 2013. Modeling of atmospheric gravity effects for high-precision observations. Int. J. Geosci. 4, 33344.

Gitlein, O., 2009. Absolutgravimetrische Bestimmung der Fennoskandischen Landhebung mit dem FG5-220, Ph.D. thesis. Leibniz Universität Hannover.

Heck, B., Mälzer, H., 1983. Determination of vertical recent crustal movements by levelling and gravity data. In: Vyskočil, P.A.M.W., Green, R. (Eds.), Recent Crustal Movements, 1982. Vol. 20 of Developments in Geotectonics. Elsevier, pp. 251–264.

Kierulf, H.P., Steffen, H., Simpson, M.J.R., Lidberg, M., Wu, P., Wang, H., 2014. A GPS velocity field for Fennoscandia and a consistent comparison to glacial isostatic adjustment models. J. Geophys. Res. 119 (8), 6613–6629.

Lambert, A., Courtier, N., James, T., 2006. Long-term monitoring by absolute gravimetry: tides to postglacial rebound. J. Geodyn. 41 (1-3), 307–317.

Leirião, S., He, X., Christiansen, L., Andersen, O.B., Bauer-Gottwein, P., 2009. Calculation of the temporal gravity variation from spatially variable water storage change in soils and aquifers. J. Hydrol. 365 (3–4), 302–309.

Lidberg, M., Johansson, J.M., Scherneck, H.-G., Milne, G., 2010. Recent results based on continuous GPS observations of the GIA process in Fennoscandia from BIFROST. J. Geodyn. 50, 8–18.

Lyard, F., Lefevre, F., Letellier, T., Francis, O., 2006. Modelling the global ocean tides: modern insights from FES2004. Ocean Dyn. 56 (5), 394–415.

Lysaker, D.I., Breili, K., Pettersen, B.R., 2008. The gravitational effect of ocean tide loading at high latitude coastal stations in Norway. J. Geod. 82 (9), 569–583.

Mäkinen, J., Virtanen, H., Bilker-Koivula, M., Ruotsalainen, H., Näränen, J., Raja-Halli, A., 2015. The Effect of Helium Emissions by a Superconducting Gravimeter on the Rubidium Frequency Standards of Absolute Gravimeters. Springer, Berlin, Heidelberg, pp. 1–6.

Müller, J., Naeimi, M., Gitlein, O., Timmen, L., Denker, H., 2012. A land uplift model in Fennoscandia combining GRACE and absolute gravimetry data. Phys. Chem. Earth, Parts ABC 53-54, 54–60.

Matsumoto, K., Takanezawa, T., Ooe, M., 2000. Ocean tide models developed by assimilating TOPEX/POSEIDON altimeter data into hydrodynamical model: a global model and a regional model around Japan. J. Oceanogr. 56 (5), 567–581.

Mazzotti, S., Lambert, A., Henton, J., James, T.S., Courtier, N., 2011. Absolute gravity calibration of GPS velocities and glacial isostatic adjustment in mid-continent North America. Geophys. Res. Lett. 38 (24.).

Micro-g LaCoste, 2012. g9 User's Manual, April 2012 version. Micro-g LaCoste, Lafayette, Colorado, USA.

Mikolaj, M., Meurers, B., Mojzeš, M., 2015. The reduction of hydrology-induced gravity variations at sites with insufficient hydrological instrumentation. Stud. Geophys. Geod. 59 (3), 424–437.

Mikolaj, M., Meurers, B., Güntner, A., 2016. Modelling of global mass effects in hydrology, atmosphere and oceans on surface gravity. Comp. Geosci. 93, 12–20.

Milne, G.A., Davis, J.L., Mitrovica, J.X., Scherneck, H.-G., Johansson, J.M., Vermeer, M., Koivula, H., 2001. Space-geodetic constraints on glacial isostatic adjustment in Fennoscandia. Science 291 (5512), 2381–2385.

Niebauer, T.M., Sasagawa, G.S., Faller, J.E., Hilt, R., Klopping, F., 1995. A new generation of absolute gravimeters. Metrologia 32 (3), 159–180.

Nordman, M., Poutanen, M., Kairus, A., Virtanen, J., 2014. Using the Nordic Geodetic Observing System for land uplift studies. Solid Earth 5 (2), 673–681.

Olesen, O., Kierulf, H.P., Brönner, M., Dalsegg, E., Fredin, O., Solbakk, T., 2013. Deep weathering, neotectonics and strandflat formation in Nordland, northern Norway. Norwegian J. Geol. 93 (3-4), 189–213.

Olsson, P.-A., Scherneck, H.-G., Ågren, J., 2009. Effects on gravity from non-tidal sea level variations in the Baltic Sea. J. Geodyn. 48 (3-5), 151–156.

Olsson, P.-A., Milne, G., Scherneck, H.-G., Ågren, J., 2015. The relation between gravity rate of change and vertical displacement in previously glaciated areas. J. Geodyn. 83, 76–84.

Pálinkáš, V., Lederer, M., Kostelecký, J., Šimek, J., Mojzeš, M., Ferianc, D., Csapó, G., 2012. Analysis of the repeated absolute gravity measurements in the Czech Republic, Slovakia and Hungary from the period 1991–2010 considering instrumental and hydrological effects. J. Geod. 87 (1), 29–42.
Penna, N.T., Bos, M.S., Baker, T.F., Scherneck, H.-G., 2008. Assessing the accuracy of predicted ocean tide loading displacement values. J. Geod. 82 (12), 893–907.
Petit, G., Luzum, B.e., 2010. IERS Conventions (2010) Tech. rep. International Earth Rotation and Reference Systems Service (IERS), Frankfurt am Main, tech. Note 36, 179 pp.
Pettersen, B.R., Bilker-Koivula, M., Breili, K., Engfeldt, A., Falk, R., Gitlein, O., Gjevestad, J.G.O., Hoppe, W., Lysaker, D.I., Mäkinen, J., Omang, O.C.D., Reinhold, A., Timmen, L., 2010. An accuracy assessment of absolute gravimetric observations in Fennoscandia. Nordic J. Surv. Real Estate Res. 7, 7–14.
Pettersen, B.R., 2011. The Postglacial Rebound Signal of Fennoscandia Observed by Absolute Gravimetry, GPS, and Tide Gauges. Int. J. Geophys, Article ID 957329.
Ray, R.D., 1999. A global ocean tide model from Topex/Poseidon altimetry: GOT99.2. Tech. rep. National Aeronautics and Space Administration (NASA), tech. Memo. 209478.
Rodell, M., Houser, P.R., Jambor, U., Gottschalck, J., Mitchell, K., Meng, C.-J., Arsenault, K., Cosgrove, B., Radakovich, J., Bosilovich, M., Entin, J.K., Walker, J.P., Lohmann, D., Toll, D., 2004. The global land data assimilation system. Bull. Am. Meteor. Soc. 85 (3), 381–394.
Roland, E., 1998. Absolutt tyngdemåling i Fennoskandia og Svalbard (Absolute gravity measurements in Fennoscandia and Svalbard), Tech. rep. Norwegian Mapping Authority, internal project report (in Norwegian), 21 pp.
Sasagawa, G., 1989. Validation and application of an absolute gravity meter in California, Ph.D. thesis. University of California, San Diego.
Savcenko, R., Bosch, W., 2011. EOT11a – a new tide model from multi-mission altimetry. In: Poster Presented at the Ocean Surface Topography Science Team Meeting, San Diego, October 19–21.
Schmerge, D., Francis, O., Henton, J., Ingles, D., Jones, D., Kennedy, J., Krauterbluth, K., Liard, J., Newell, D., Sands, R., Schiel, A., Silliker, J., Westrum, D., 2012. Results of the first North American comparison of absolute gravimeters, NACAG-2010. J. Geod. 86 (8), 591–596.
Schwiderski, E.W., 1980. On charting global ocean tides. Rev. Geophys. 18 (1), 243–268.
Simpson, M.J.R., Breili, K., Kierulf, H.P., 2013. Estimates of twenty-first century sea-level changes for Norway. Clim. Dyn. 42 (5), 1405–1424.
Šprlák, M., Gerlach, C., Pettersen, B.R., 2015. Validation of global gravitational field models in Norway. Newton's Bull. 5, 3–12.
Steffen, H., Wu, P., 2011. Glacial isostatic adjustment in Fennoscandia – a review of data and modeling. J. Geodyn. 52 (3-4), 169–204.
Steffen, H., Gitlein, O., Denker, H., Müller, J., Timmen, L., 2009. Present rate of uplift in Fennoscandia from GRACE and absolute gravimetry. Tectonophysics 474 (1-2), 69–77.
Timmen, L., Gitlein, O., Klemann, V., Wolf, D., 2011. Observing gravity change in the Fennoscandian uplift area with the hanover absolute gravimeter. Pure Appl. Geophys. 169 (8), 1331–1342.
Timmen, L., Engfeldt, A., Scherneck, H.-G., 2015. Observed secular gravity trend at Onsala station with the FG5 gravimeter from Hannover. J. Geod. Sci. 5, 1–8.
Timmen, L., 2010. Absolute and Relative Gravimetry. In: Sciences of Geodesy – I: Advances and Future Directions. Springer, Berlin, Heidelberg, pp. 1–48.
Torge, W., Müller, J., 2012. Geodesy. Walter de Gruyter, Berlin.
Van Camp, M., Williams, S.D.P., Francis, O., 2005. Uncertainty of absolute gravity measurements. J. Geophys. Res. 110 (B5.).
Van Camp, M., de Viron, O., Scherneck, H.-G., Hinzen, K.-G., Williams, S.D.P., Lecocq, T., Quinif, Y., Camelbeeck, T., 2011. Repeated absolute gravity measurements for monitoring slow intraplate vertical deformation in western Europe. J. Geophys. Res. 116 (B8.).
Van Camp, M., de Viron, O., Avouac, J.P., 2016. Separating climate-induced mass transfers and instrumental effects from tectonic signal in repeated absolute gravity measurements. Geophys. Res. Lett. 43, 4313–4320.
Vestøl, O., 2006. Determination of postglacial land uplift in fennoscandia from leveling, tide-gauges and continuous gps stations using least squares collocation. J. Geod. 80 (5), 248–258.
Virtanen, H., Tevo, M., Bilker-Koivula, M., 2006. Comparison of superconducting gravimeter observations with hydrological models of various spatial extents. In: Bull. d'Inf. Marées Terr, pp. 11361–11368.
Wahr, J., DaZhong, H., Trupin, A., 1995. Predictions of vertical uplift caused by changing polar ice volumes on a viscoelastic Earth. Geophys. Res. Lett. 22 (8), 977–980.
Wunsch, C., Stammer, D., 1997. Atmospheric loading and the oceanic inverted barometer effect. Rev. Geophys. 35 (1), 79–107.